



Cohabitation reaction–diffusion model for virus focal infections



Daniel R. Amor^{a,b,*}, Joaquim Fort^c

^a ICREA-Complex Systems Lab, Universitat Pompeu Fabra, Dr. Aiguader 80, 08003, Barcelona, Spain

^b Institut de Biologia Evolutiva, CSIC-UPF, Psg Barceloneta, Barcelona, Spain

^c Complex Systems Lab, Departament de Física, Universitat de Girona, 17071 Girona, Catalonia, Spain

HIGHLIGHTS

- We report an inaccuracy in classical reaction–diffusion models for virus infections.
- We present a new model preventing virion diffusion during intracellular replication.
- Our model yields better results than nondelayed models for two T7 virus strains.
- The predicted infection speed saturates for high values of the virus adsorption rate.
- The predicted infection speed is highly dependent on the death rate of infected cells.

ARTICLE INFO

Article history:

Received 28 March 2014

Received in revised form 4 July 2014

Available online 3 September 2014

Keywords:

Population dynamics

Driven diffusive systems

Nonlinear dynamics

ABSTRACT

The propagation of virus infection fronts has been typically modeled using a set of classical (noncohabitation) reaction–diffusion equations for interacting species. However, for some single-species systems it has been recently shown that noncohabitation reaction–diffusion equations may lead to unrealistic descriptions. We argue that previous virus infection models also have this limitation, because they assume that a virion can simultaneously reproduce inside a cell and diffuse away from it. For this reason, we build a several-species cohabitation model that does not have this limitation. Furthermore, we perform a sensitivity analysis for the most relevant parameters of the model, and we compare the predicted infection speed with observed data for two different strains of the T7 virus.

© 2014 Elsevier B.V. All rights reserved.

1. Introduction

Reaction–diffusion fronts have many applications in Physics, Biology and cross-disciplinary topics [1–4]. Some purely physical examples are superconducting fronts [5] and combustion flames [6]. In this paper we consider a biophysical application, namely the spread of virus infections in a cell culture [7–11]. Very recently, the importance of this research in the context of virus treatments of cancer tumors has been stressed [12]. This interest is due to the fact that some viruses can selectively kill tumor cells and therefore be used in medical treatments of cancer tumors [12]. Therefore, understanding the spatial speed of virus infections is not only a relevant biological phenomenon, but also has potentially relevant clinical applications.

In focal infections a cell in a culture is infected by a virion (i.e., a single virus particle). The virion reproduces inside the cell. Some time later, a new generation of virions leaves the cell, they diffuse away and infect other cells. This cycle is repeated

* Corresponding author at: ICREA-Complex Systems Lab, Universitat Pompeu Fabra, Dr. Aiguader 80, 08003 Barcelona, Spain. Tel.: +34 933160531.
E-mail address: daniel.rodriguez-amor@upf.edu (D.R. Amor).

many times and a region of dead cells (a plaque) grows at a constant speed, which can be measured experimentally. The propagation of such focal infections has been modeled mathematically [7,13–15]. The interactions between the three species in the system can be summarized as follows



where V , B and I refer to virus, uninfected cells, and infected cells, respectively. k_1 stands for the adsorption rate of a virion into a uninfected cell (the latter is sometimes called the host). k_2 is the rate for the death (or lysis) of an infected cell, a process that releases y new viruses into the extracellular medium (y is called the yield). In the case of cells, diffusion does not take place because cells are immobilized in agar. Thus, the evolution of B and I is governed only by reaction (i.e., population growth) effects, which are well described by the following two equations [7,13–15]

$$\frac{\partial B(r, t)}{\partial t} = -k_1 B(r, t) V(r, t), \quad (2)$$

$$\frac{\partial I(r, t)}{\partial t} = k_1 V(r, t) B(r, t) - k_2 I(r, t). \quad (3)$$

In Eqs. (2) and (3) r is the radial coordinate (distance to the point where the virus was first inoculated), and the symbols $[\dots]$ denote concentration.¹ In contrast to cells, virions are able to diffuse within the extracellular medium. Furthermore, the delay or lag time T that the virions need to replicate inside the infected cell has been shown to be critically important in order to predict realistic infection speeds [7,14]. In previous models, these features of the virus population were studied by means of the following time-delayed reaction–diffusion equation [7,13,14]

$$\frac{\partial V(r, t)}{\partial t} + \frac{T}{2} \frac{\partial^2 V(r, t)}{\partial t^2} = D_{\text{eff}} \frac{\partial^2 V(r, t)}{\partial r^2} + F(r, t) + \frac{T}{2} \frac{\partial F(r, t)}{\partial t} \Big|_g, \quad (4)$$

where F is called the virus growth function, that reads:

$$F(r, t) \equiv \frac{\partial V(r, t)}{\partial t} \Big|_g = -k_1 V(r, t) B(r, t) + k_2 y I(r, t). \quad (5)$$

In Eqs. (4) and (5), the subindex $|_g$ remarks that the corresponding time derivatives must take into account growth effects, but not diffusion (see Ref. [16] for a detailed discussion on this point). Moreover, in Eq. (4) we have applied the effective diffusion coefficient D_{eff} , which takes into account the effects of the actual hindered diffusion. In this sense, D_{eff} introduces the corresponding diffusion corrections due to the presence of spheroids (host bacteria) in the medium in which the viruses diffuse. The relation between D_{eff} and the virus diffusivity D in the continuous medium (in our case agar) is given by the Fricke's equation [17]:

$$D_{\text{eff}} = \frac{1 - f}{1 + \frac{f}{x}} D, \quad (6)$$

where $f = B_0/B_{\text{max}}$ is the initial concentration of bacteria in the experiment relative to its maximum possible value, and x takes care of the shape of the suspended particles (host bacteria). In this paper we will consider the *E. coli* species, for which the shape factor $x = 1.67$ was derived in Ref. [7].

In recent years, single-species reaction–diffusion models have been modified to take into account the cohabitation effect, namely the fact that for some biological species (e.g. humans) newborn individuals cannot disperse away from their parents until a delay time after their birth [18]. Mathematically this leads to a different kind of reaction–diffusion equation, in which the contributions of biological reproduction and dispersal are not added up but computed as separate steps (for example, first reproduction and later dispersal). Clearly, this effect takes place also in virus infections, because it is well-known that after a virus enters a cell, the new generation of viruses does not leave the cell until after a delay time corresponding to the death of the host cell. In the present paper, we build a model that takes this cohabitation effect into account for virus infections. We will also apply it to describe additional experimental data to those analyzed in previous papers [7,13,14].

2. Cohabitation model

Typically, models for virus focal infections are either based in Eq. (4) [7,13,14], or in its classical nondelayed version [15,19], namely Eq. (4) with $T = 0$ (i.e., Fisher's equation). Before modifying Eq. (4), we need first to recall that it can be derived from the following integro–difference reaction–dispersal equation [20,21]

$$\begin{aligned} V(x, y, t + T) - V(x, y, t) &= \iint V(x + \Delta_x, y + \Delta_y, t) \phi_T(\Delta_x, \Delta_y) d\Delta_x d\Delta_y \\ &\quad - V(x, y, t) + R_T[V(x, y, t)] - V(x, y, t), \end{aligned} \quad (7)$$

¹ An additional, quadratic term has been sometimes added to Eq. (3) in order to describe the so-called one-step experiments [7,14] but is not necessary for the purposes of the present paper, because we are here concerned with the front speed, which is derived by linearizing the reaction–diffusion equations.

where, for simplicity, we have omitted the symbols [...] for the virus concentration. In Eq. (7) the dispersal kernel $\phi_T(\Delta_x, \Delta_y)$ gives the probability that a virion initially at position $(x + \Delta_x, y + \Delta_y)$ moves to (x, y) after a generation time T . Accordingly, the first and second terms on the right hand side (RHS) of Eq. (7) compute the variation of virus concentration due to the virions arriving and leaving a unit area centered at (x, y) [20]. The last two terms in Eq. (7) give the increase in virus concentration due to net population number growth (reproduction minus death) according to the following definition [20, 21]

$$R_T[V(x, y, t)] \equiv V(x, y, t) + TF(x, y, t) + \frac{T^2}{2} \left. \frac{\partial F(x, y, t)}{\partial t} \right|_g + \dots \tag{8}$$

A Taylor expansion, up to second order in space, of the first term on the RHS of Eq. (7) yields

$$\iint V(x + \Delta_x, y + \Delta_y, t) \phi_T(\Delta_x, \Delta_y) d\Delta_x d\Delta_y \simeq V(x, y, t) + TD_{\text{eff}} \nabla^2 V(x, y, t), \tag{9}$$

where, as usual, the diffusion coefficient is $D_{\text{eff}} \equiv \frac{1}{4T} \iint \Delta^2 \phi(\Delta) d\Delta_x d\Delta_y = \frac{\langle \Delta^2 \rangle}{4T}$ [20] and we have made use of the Laplacian operator $\nabla^2 \equiv \left(\frac{\partial^2}{\partial x^2} + \frac{\partial^2}{\partial y^2} \right)$. Moreover, we have considered an isotropic kernel such that $\phi(\Delta_x, \Delta_y) = \phi(\Delta)$, with $\Delta^2 = \Delta_x^2 + \Delta_y^2$. By Taylor-expanding Eq. (7) up to second order in space and time, and making use of Eqs. (8)–(9), we obtain Eq. (4). This summarizes a derivation in Ref. [20]. We can now explain how to modify this derivation in order to take into account the cohabitation effect.

Eq. (7) considers reproduction and dispersal as two separate processes. However, this separation of events is not always realistic when modeling biophysical systems, thus the following so-called cohabitation equation has been proposed for single-species systems [18,21]

$$V(x, y, t + T) = R_T \left[\iint V(x + \Delta_x, y + \Delta_y, t) \phi(\Delta_x, \Delta_y) d\Delta_x d\Delta_y \right]. \tag{10}$$

In our case (virus infections), it is very important to note that in noncohabitation models (Eq. (7)) the virus population number at time t is used to compute both the diffusion and the reaction components that lead to the virus number distribution at time $t + T$. Fig. 1 graphically shows that this approach leads to an unrealistic description of the virus dynamics. Consider that the virus population number is concentrated at a given region (let us assume a one-dimensional discrete space that permits a specially clear and visual interpretation of the phenomena). As indicated in the left hand side in Fig. 1, we assume that at time t a given population number $V^* > 0$ is occupying this central region, so that the virus number at the nearest left neighbor, the central region and the nearest right neighbor, is respectively depicted by the bracket $(0, V^*, 0)$ (i.e., no virus are present at the neighbor regions). In the noncohabitation model, the diffusion is computed from the original number profile $(0, V^*, 0)$ at time t , giving rise to the number profile (V_d^*, V_{-d}^*, V_d^*) (where $2V_d^* + V_{-d}^* = V^*$, since the diffusion process conserves the total virus mass). Additionally, the virus reactions are also computed from $(0, V^*, 0)$. The profile $(0, V^*, 0)$ determines the number of cell infections at time t , and the resulting virus net reproduction is denoted by $(0, gV^*, 0)$ (where we arbitrarily consider g as the corresponding virus net reproduction rate). Note that the noncohabitation model adds up the diffusion and the reproduction processes, which leads to the virus number profile $(V_d^*, gV^* + V_{-d}^*, V_d^*)$ at time $t + T$. The contradiction is now clear, since the model does not consider that some viruses may reproduce at their final locations (instead the model arbitrarily assumes that all new viruses must appear at the initial location). In contrast, when we compute the virus dynamics using the cohabitation model no contradictions of this kind are observed. As shown in Fig. 1, the virus number $(V_d^*, V_{-d}^*, V_d^*) \cdot (1 + g)$ at time $t + T$ results from a sequential computation of the events: first the diffusion effect is considered and then the reproduction is computed over the already diffused virus (i.e. over the newly distributed profile (V_d^*, V_{-d}^*, V_d^*)). Obviously, the same final result is obtained if viruses first reproduce (i.e., $(0, V^*, 0) \Rightarrow (0, (1 + g)V^*, 0)$) and then diffuse. Thus, the cohabitation Eq. (10) provides a better mathematical description of biological reality than the noncohabitation Eq. (7), used in previous work [7,13,14].

Let us now focus on the RHS of Eq. (10). In order to take into account the effects of population growth after dispersion, let us designate with the symbol $|_g$ the time derivatives associated to population growth.³ Similarly to Eq. (8), by Taylor-expanding the RHS of Eq. (10) up to second order in time we obtain

$$R_T \left[\iint V(x + \Delta_x, y + \Delta_y, t) \phi_T(\Delta_x, \Delta_y) d\Delta_x d\Delta_y \right] = \iint V(x + \Delta_x, y + \Delta_y, t) \phi_T(\Delta_x, \Delta_y) d\Delta_x d\Delta_y + TF_c(x, y, t) + \frac{T^2}{2} \left. \frac{\partial F_c(x, y, t)}{\partial t} \right|_g + \dots \tag{11}$$

² We use the factor $(1 + g)$ rather than g for the following reason. Without diffusion, the non-cohabitation model (upper row in Fig. 1) yields $(0, gV^*, 0) + (0, V^*, 0) = (0, (1 + g)V^*, 0)$. For the cohabitation model (lower row in Fig. 1) to agree with this without diffusion, reproduction must be computed using $(1 + g)$, not g .

³ A more detailed explanation about the significance of the subindex $|_g$ on noncohabitation, reaction–diffusion equations for focal infections can be found in Ref. [14].

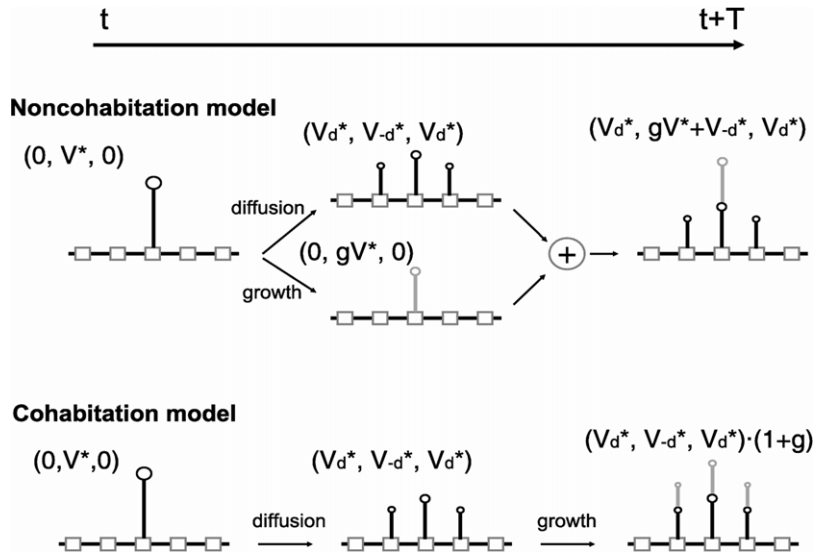


Fig. 1. Comparison of the reaction–diffusion algorithms of the noncohabitation and the cohabitation model. At time $t + T$, a different virus number profile is obtained from each model. The cohabitation model is the more realistic because the diffusion and growth processes are computed sequentially. Instead the noncohabitation model assumes that all new viruses appear at the initial location. Note that the final number of viruses is the same in both models, namely $(1 + g)V^*$ (because diffusion conserves the mass, so $V_d^* + V_{-d}^* + V_d^* = V^*$).

where F_c corresponds to the growth function for the cohabitation model, which according to Eq. (5) is given by

$$\begin{aligned}
 F_c(x, y, t) &= \frac{\partial}{\partial t} \iint V(x + \Delta_x, y + \Delta_y, t) \phi_T(\Delta_x, \Delta_y) d\Delta_x d\Delta_y \Big|_g \\
 &= -k_1 B(x, y, t) \iint V(x + \Delta_x, y + \Delta_y, t) \phi_T(\Delta_x, \Delta_y) d\Delta_x d\Delta_y + k_2 y I(x, y, t),
 \end{aligned}
 \tag{12}$$

where we have omitted brackets for notational simplicity. The second line in Eq. (12) states that viruses that reached position (x, y) by dispersal (at time t) will infect cells (that are located at (x, y)) at rate k_1 . It is also worth to remark that $\phi(0, 0)$ takes into account the fraction of viruses which were already at (x, y) and can infect cells because they did not diffuse at time t . Now, we can perform a second-order Taylor expansion in space in the second line of Eq. (12), thus simplifying the growth function into

$$F_c(x, y, t) \simeq -k_1 B(x, y, t) (V(x, y, t) + T D_{\text{eff}} \nabla^2 V(x, y, t)) + k_2 y I(x, y, t).
 \tag{13}$$

Finally, taking into account Eq. (11), a Taylor expansion of Eq. (10) up to second order in time gives the following cohabitation reaction–diffusion equation

$$\frac{\partial V(r, t)}{\partial t} + \frac{T}{2} \frac{\partial^2 V(r, t)}{\partial t^2} = D_{\text{eff}} \nabla^2 V(r, t) + F_c(r, t) + \frac{T}{2} \frac{\partial F_c}{\partial t} \Big|_g,
 \tag{14}$$

where F_c is given by Eq. (13). For convenience, we have expressed Eq. (14) in radial coordinates, which are specially useful to describe the spread of focal infections.⁴ This model is completed with the evolution equations for uninfected cells and infected cells we presented in the introduction, namely

$$\frac{\partial B(r, t)}{\partial t} = -k_1 B(r, t) V(r, t),
 \tag{15}$$

$$\frac{\partial I(r, t)}{\partial t} = k_1 V(r, t) B(r, t) - k_2 I(r, t).
 \tag{16}$$

In the rest of this paper, we derive the infection speed according to the cohabitation model (14)–(16) and compare it to the observed data for several virus strains.

⁴ The conversion from Cartesian to radial coordinates for the Laplacian is $\nabla^2[V](x, y, t) = \frac{\partial^2[V](x, y, t)}{\partial x^2} + \frac{\partial^2[V](x, y, t)}{\partial y^2} = \frac{1}{r} \frac{\partial}{\partial r} \left(r \frac{\partial[V](r, t)}{\partial r} \right) = \frac{1}{r} \frac{\partial[V](r, t)}{\partial r} + \frac{\partial^2[V](r, t)}{\partial r^2}$. However, in this paper we are interested in the asymptotic front speed ($r \rightarrow \infty$ and $t \rightarrow \infty$) of focal infections. This has allowed to simply consider $\nabla^2[V](r, t) = \frac{\partial^2[V](r, t)}{\partial r^2}$ in all the computations of the front speeds in this paper.

3. Infection front speed

In this section we focus on the derivation of the infection speed that results from the cohabitation model. For this purpose it is necessary to solve the set of evolution equations (14)–(16). In this sense, it is practical to rewrite the equations in terms of dimensionless variables $\bar{B} \equiv [B]/B_0$, $\bar{V} \equiv [V]/B_0$, $\bar{I} \equiv [I]/B_0$, $\bar{t} \equiv k_2 t$, and $\bar{r} \equiv r\sqrt{k_2/D_{\text{eff}}}$ and dimensionless parameters $\bar{\tau} \equiv k_2 \tau$, $\kappa \equiv k_1 B_0/k_2$, where B_0 is the initial concentration of bacteria. Then, the set (14)–(16) becomes

$$\frac{\bar{\tau}}{2}\bar{V}_{\bar{t}\bar{t}} + \bar{V}_{\bar{t}} = \bar{V}_{\bar{r}\bar{r}} + \bar{F} - \frac{\bar{T}}{2}\kappa\bar{B}_{\bar{t}}(\bar{V} + \bar{T}\bar{V}_{\bar{r}\bar{r}}) - \frac{\bar{T}}{2}\kappa\bar{F}\bar{B} + \frac{\bar{\tau}}{2}y\bar{I}_{\bar{t}} \quad (17)$$

$$\bar{B}_{\bar{t}} = -\kappa\bar{V}\bar{B} \quad (18)$$

$$\bar{I}_{\bar{t}} = \kappa\bar{V}\bar{B} - \bar{I}, \quad (19)$$

where the dimensionless growth function corresponds to

$$\bar{F} = -\kappa\bar{B}(\bar{V} + \bar{T}\bar{V}_{\bar{r}\bar{r}}) + y\bar{I}. \quad (20)$$

For simplicity, in Eqs. (17)–(20) we have used the notation $\bar{V}_{\bar{t}}$, $\bar{B}_{\bar{t}}$ and $\bar{I}_{\bar{t}}$ to indicate, respectively, the partial time derivatives of \bar{V} , \bar{B} and \bar{I} (accordingly, $\bar{V}_{\bar{t}\bar{t}}$ and $\bar{V}_{\bar{r}\bar{r}}$ stand for the corresponding second partial derivatives of \bar{V}). Furthermore, we have also omitted the space and time dependences of the dimensionless population densities and the growth function (i.e., $\bar{V}(\bar{r}, \bar{t})$, $\bar{B}(\bar{r}, \bar{t})$, $\bar{I}(\bar{r}, \bar{t})$ and $\bar{F}(\bar{r}, \bar{t})$) appear as \bar{V} , \bar{B} , \bar{I} and \bar{F} .

As usual [4], we look for constant-shape solutions depending only on the new variable $\bar{z} \equiv \bar{r} - \bar{c}\bar{t}$, where $\bar{c} > 0$ is the dimensionless wave front speed (so the dimensional speed is $c = \bar{c}\sqrt{k_2 D_{\text{eff}}}$), and we linearize our Eqs. (17)–(20) around the unstable steady state $(V, B, I) = (0, B_0, 0)$, i.e., $(\bar{V}, \bar{B}, \bar{I}) = (\epsilon_V, 1 - \epsilon_B, \epsilon_I)$, where $\vec{\epsilon} = (\epsilon_V, \epsilon_B, \epsilon_I) = \vec{\epsilon}_0 \exp(-\lambda\bar{z})$. For non-trivial solutions $(\epsilon_V, \epsilon_B, \epsilon_I) \neq (0, 0, 0)$ to exist, the determinant of the matrix corresponding to the linearized set of three evolution equations must vanish. This condition leads to the following characteristic equation

$$\begin{aligned} & \lambda^3 \bar{c} \left(-\frac{\bar{T}^2}{2} \kappa^2 + \bar{T} \left(\kappa + \frac{\bar{c}^2}{2} \right) - 1 \right) + \lambda^2 \left(\bar{T} \left(-\frac{\bar{T}}{2} \kappa^2 + \kappa + \frac{\bar{c}^2}{2} \right) + \bar{c}^2 - 1 \right) \\ & + \lambda \bar{c} \left(\frac{\bar{T}}{2} \kappa (-\kappa - y) + \kappa + 1 \right) + \kappa \left(\frac{\bar{T}}{2} \kappa (y - 1) - y + 1 \right) = 0. \end{aligned} \quad (21)$$

Finally, the wave front speed can be calculated numerically from the marginal stability condition [22]. For reaction–diffusion equations with reactive terms that can be linearized (“pulled” fronts), Aronson and Weinberger [23] proved rigorously that every initial condition that decays spatially at least as fast as $\exp(-\lambda x)$, with $\lambda = c_{\text{min}}/2$, approaches for large times the smallest possible velocity c_{min} . In practice, one usually assumes that initially the population density is zero everywhere except in a finite region, where it is equal to its maximum possible value (carrying capacity), i.e. that the initial profile is a Heaviside step function. This is biologically reasonable, and then the work by Aronson and Weinberger [23] summarized above implies that the front propagates at the minimum speed. This is called the linear marginal stability criterion (see also Ref. [22]). Usually numerical simulations also use a Heaviside step function as initial condition. Their results agree with the linear marginal stability criterion, not only for single reaction–diffusion equations but also for higher-order equations [24] as well as for systems of equations [14]. In agreement with these (and many other) previous results, we apply here the linear marginal stability criterion, i.e. we assume that the front approaches for large times the smallest possible velocity. Thus, from Eq. (21) we obtain the infection front speed:

$$\bar{c} = \min_{\lambda > 0} [\bar{c}(\lambda)]. \quad (22)$$

4. Application to T7 infections: cohabitation front speed versus observed data

In this section we present some results of the cohabitation model presented above, for some specific cases of T7 focal infections.

In 1993, J. Yin published the frequencies observed for the infection speeds of T7 strains when repeating focal infection experiments under the same laboratory conditions [25]. The experiments were performed with several strains of the T7 virus infecting *Escherichia coli* cells. In this section we compare the observed infection speeds for two specific strains (namely, the wild strain and the p001⁵ mutant) of the T7 virus [25] with the infection speed predicted by our cohabitation model (Eq. (22)) and some previous models by other authors [15].

⁵ There are also data for another T7 mutant (p005), but we do not include them because they are very similar to those for the p001 strain.

Eq. (1) summarizes the interactions between the species in a focal infection system. Accordingly, both the adsorption rate k_1 and death rate k_2 are relevant parameters. Since the other parameters in this system have been measured more precisely [7], we focus on the effect of the rates k_1 and k_2 . We analyze the influence of both parameters as follows. The mean value and the associated standard error for both k_1 ⁶ and k_2 (see below) has been determined from the observed data. From the mean value of \bar{k}_i (in this case, $i = 1, 2$) and the associated standard error σ_i the normal (i.e. Gaussian) distribution for the values of k_i is

$$f(k_i) = \frac{1}{\sigma_i \sqrt{2\pi}} \text{Exp} \left(-\frac{(k_i - \bar{k}_i)^2}{2\sigma_i^2} \right). \quad (23)$$

According to statistical theory, integrating $f(k_i)$ within a specific range of k_i gives the probability that the empirical value of k_i lays within such specific range. For example, it is well known that the probability that the empirical value of k_i lays between \bar{k}_i and $\bar{k}_i + \sigma_i$ is approximately 34.1%. In order to evaluate the results from the cohabitation model (Eq. (22)) and to reveal the influence of the parameters k_1 and k_2 on the infection speed, we follow two steps:

1. We first compute the infection speed for several values of k_i ($i = 1, 2$) in the range⁷ $\{\bar{k}_i - 3\sigma_i, \bar{k}_i + 3\sigma_i\}$, without varying the values of the other independent parameters (namely k_j (with $j \neq i$), y , D_{eff} and B_0). In the special case of k_2 , let us note that the value of T is not independent from k_2 , and must be varied accordingly to variations in k_2 (see below).
2. To the speed ranges computed in step 1, we assign probabilities by integrating the Gaussian distribution (23). For example, given the front speed range $\{c(\bar{k}_i - \sigma_i), c(\bar{k}_i)\}$ (computed from Eq. (22) by using the values $k_i = \bar{k}_i - \sigma_i$ and $k_i = \bar{k}_i$) we assign the probability $\int_{\bar{k}_i - \sigma_i}^{\bar{k}_i} f(k_i) dk_i = 34.1\%$ for the speed to lay within this speed range.

The values for the death rate k_2 have been obtained by using the procedure detailed in Ref. [7] and one-step growth experimental data. In one-step growth experiments, the system is initially composed by a layer of infected cells (without free virus in the extracellular medium). As explained in previous works, the evolution of the concentration of free viruses in such experiments shows the logistic behavior:

$$V(t) = \frac{V_{\text{MAX}}}{c_1 \exp[-k_2 t] + 1}, \quad (24)$$

where V_{MAX} corresponds to the maximum concentration of virus (i.e., the concentration observed when $t \rightarrow \infty$), and c_1 is a constant that depends on the initial conditions. The value of k_2 has been obtained from the best fit of Eq. (24) to one-step growth data from Fig. 3 in Ref. [25]. For the wild strain we obtained $\bar{k}_2 = 1.39 \text{ min}^{-1}$ and $\sigma_2 = 0.32 \text{ min}^{-1}$. For the p001 strain we obtained $\bar{k}_2 = 0.703 \text{ min}^{-1}$ and $\sigma_2 = 0.085 \text{ min}^{-1}$.

As proposed in Ref. [7], we compute the delay time as the interval T that satisfies the condition $V(T) = V_{\text{MAX}}/2$, according to Eq. (24). This leads to different delay times for each of the considered strains of the T7. For example, by taking into account the corresponding mean value of \bar{k}_2 in the previous paragraph, we obtained $T = 18.4 \text{ min}$ for the wild strain, and $T = 17.05 \text{ min}$ for the p001 strain. It is worth to note that, given that both V_{MAX} and c_1 in Eq. (24) are constants, k_2 and T are not independent parameters. Accordingly, for each value of k_2 used to generate the histograms in Fig. 2(a) and (b), we computed the corresponding delay T which satisfied the condition $V(T) = V_{\text{MAX}}/2$ in Eq. (24).

Another very relevant parameter to determine the infection front speed is D_{eff} . Its value depends on the host fraction $f = B_0/B_{\text{max}}$. Yin and co-workers did not measure directly B_0 , B_{max} or f . However, they estimated the value of f by noting that higher concentrations of nutrient led to higher values for the initial concentration of cells B_0 (before the inoculation of the virus). Thus they assumed that the value of B_0 is proportional to the concentration of nutrient [15]. They also observed that for a concentration of nutrient of 50 g/l the cells filled the volume [15]. Since in the experiments used here the concentration of nutrient was 10 g/l, their approach yields $f = 10/50 = 0.2$ [15]. Then, the value of D_{eff} is easily computed from the diffusivity of virions in agar $D = 4 \cdot 10^{-8} \text{ cm}^2/\text{s}$ [7]. Applying Eq. (6) we obtain the value $D_{\text{eff}} = 1.03 \cdot 10^{-2} \text{ mm}^2/\text{h}$, that we use below to compare the results from several models to available experimental data on the front speed of the T7 virus.

Fig. 2 presents the results of analyzing the effect of the death rate k_2 on the front speed predicted by the cohabitation model (gray shaded columns), for mean values of the other parameters. The full black columns correspond to the frequencies of observed infection speeds [25]. Fig. 2(a) presents the results for the wild strain of the T7 virus infecting *E. coli*. When comparing the histogram for the cohabitation front speed (gray shaded columns) with the observed histogram (black columns), we find remarkably good agreement. There are some differences between the observed speeds (the most frequent one is about 0.19 mm/h) and those predicted by our model (the most probable speed is that predicted by the mean value of k_2 , namely $c(\bar{k}_2) \simeq 0.25 \text{ mm/h}$). However, these differences are substantially smaller for our model than for the classical model by Yin and McCaskill (YM) [15] (Fig. 2(a)). The YM model makes use of the set of reaction–diffusion equations (2)–(5)

⁶ The mean value and the standard error of k_1 for the wild strain of the T7 virus was derived in Ref. [7] from experimental data. Since we are not aware of experimental data from which we could derive the value of k_1 for the p001 strain, but it is a mutant of the same virus, in this paper we have used the values $\bar{k}_1 = 1.29 \cdot 10^{-9} \text{ ml/min}$ and $\sigma_1 = 0.59 \cdot 10^{-9} \text{ ml/min}$ (which correspond to the values derived in Ref. [7]).

⁷ According to statistical theory, the empirical value of k_i lays into the range $\{\bar{k}_i - 3\sigma_i, \bar{k}_i + 3\sigma_i\}$ with probability of 99.7% (this probability is found when integrating $f(k_i)$ within this range).

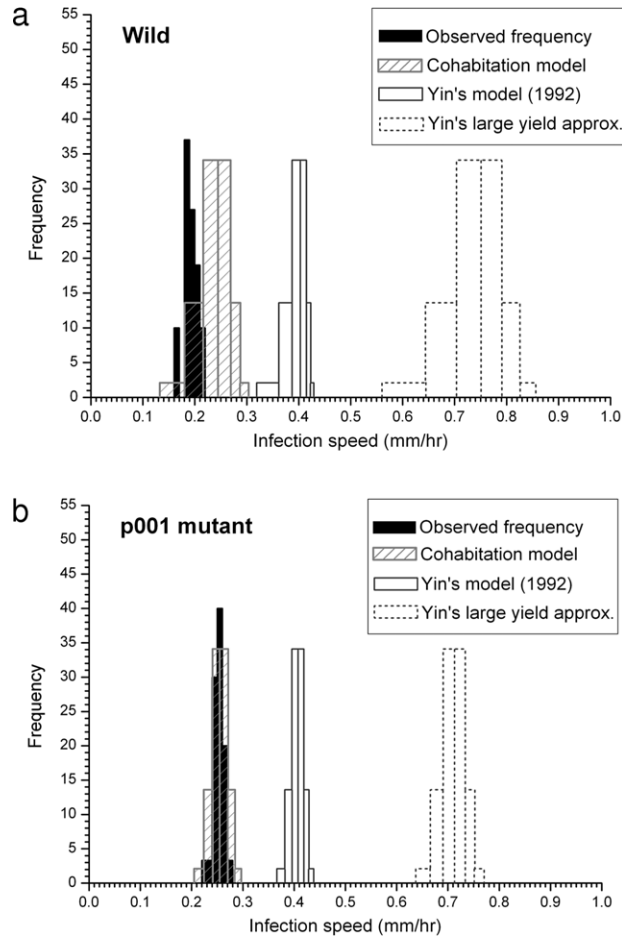


Fig. 2. Infection speed probabilities according to experiments (black columns), and for several reaction–diffusion models using the range $k_2 \in k_2 - 3\sigma_2, k_2 + 3\sigma_2$. Results from the following three models are shown: cohabitation model, the Yin and McCaskill (YM) model, and the large-yield approximation to the YM model. (a) Infection speed histograms for the wild strain of the T7 virus. The other parameter values are $k_2 = 1.39 \text{ min}^{-1}$, $\sigma_2 = 0.32 \text{ min}^{-1}$, $k_1 = 1.29 \cdot 10^{-9} \text{ ml/min}$, $f = 0.2$, $D_{\text{eff}} = 1.03 \cdot 10^{-2} \text{ mm}^2/\text{h}$, $y = 34.5$ [26], and $B_0 = 2 \cdot 10^6/\text{ml}$ [25]. (b) Infection speed histograms for the p001 strain of the T7 virus. The other parameter values are $k_2 = 0.703 \text{ min}^{-1}$, $\sigma_2 = 0.085 \text{ min}^{-1}$, $k_1 = 1.29 \cdot 10^{-9} \text{ ml/min}$, $D_{\text{eff}} = 1.03 \cdot 10^{-2} \text{ mm}^2/\text{h}$, $y = 55.4$ [26], and $B_0 = 2 \cdot 10^6/\text{ml}$ [25].

with $T = 0$ (i.e., it deals with nondelayed reaction–diffusion equations).⁸ Thus, besides the cohabitation effect (Fig. 1), the main difference between the cohabitation and the YM models is the delay time T the virion remains inside the host cell. The exact solution of the YM model is shown by empty columns in Fig. 2(a), whereas the speed from the large-yield approximate solution (also proposed by YM in Ref. [15]) is shown as empty columns with dashed edges. For both solutions to the classical model, the theoretical speeds have been computed by using the same parameter values as for the cohabitation histogram. We observe that the classical model predicts substantially faster speeds than those measured experimentally the histograms from the YM models do not overlap at all with the observed histogram in Fig. 2(a). Moreover, the most probable value for the YM speed exceeds the most frequently observed value by a factor of 2 (a factor of 4 if we use the large-yield approximation). Thus, we conclude that the cohabitation model produces remarkably more realistic results than classical, noncohabitation models. This conclusion is reinforced by considering infection fronts of the p001 strain of the T7 virus (Fig. 2(b)). In this case the parameters k_2 , σ_2 and y are different than for the wild strain (see the text below Eq. (24) and the caption to Fig. 2), and the observed speed histogram (black columns in Fig. 2(b)) is also different than for the wild strain (black columns in Fig. 2(a)). Remarkably, for the p001 mutant the cohabitation model produces results that agree very well with the observed histogram (note the overlapping between the theoretical histogram and the observed one in Fig. 2(b)). In contrast, classical front speeds (for both the exact and the approximate YM solutions) are too fast to agree with the observed spread rates (black columns in Fig. 2(b)).

⁸ The original equations for the virus–host system in Ref. [15] contain an additional term for the desorption of virions from their host. However, the desorption rate constant k_{-1} is generally not significant in comparison with k_1 . As a result, the desorption rate does not appear in more recent models of the same authors [19]. Accordingly, the original terms containing k_{-1} have been omitted in Eqs. (2)–(5).

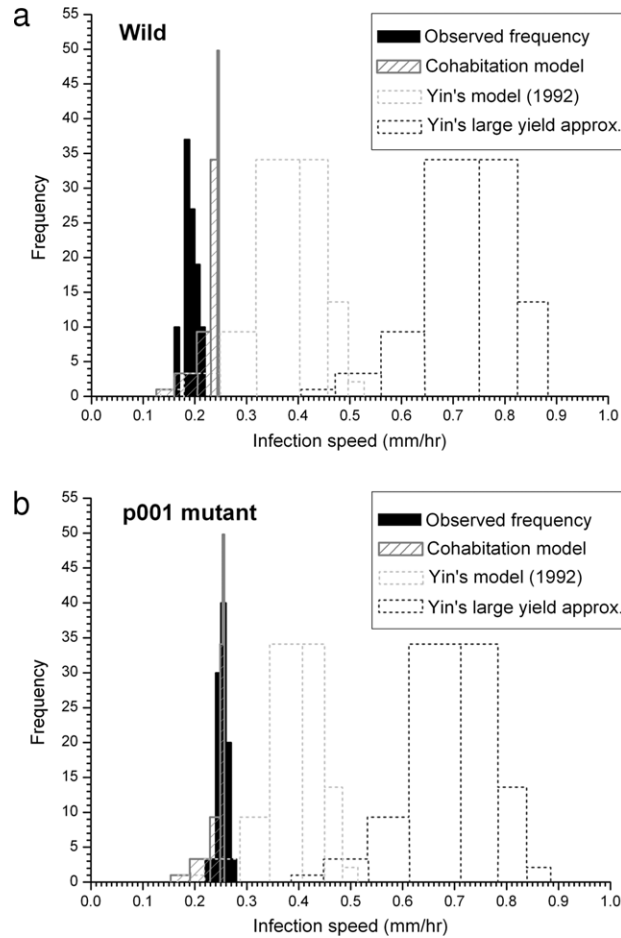


Fig. 3. Infection speed probabilities according to experiments (black columns), and several reaction–diffusion models using the range $k_1 \in k_1 - 2\sigma_1, k_1 + 3\sigma_1$. Results from the following three models are shown: cohabitation model, the Yin and McCaskill (YM) model, and the large-yield approximation to the YM model. (a) Infection speed histograms for the wild strain of the T7 virus. The other parameter values are $k_1 = 1.29 \cdot 10^{-9}$ ml/min, $\sigma_1 = 0.59 \cdot 10^{-9}$ ml/min, $k_2 = 1.39 \text{ min}^{-1}$, $f = 0.2$, $D_{\text{eff}} = 1.03 \cdot 10^{-2}$ mm²/h, $y = 34.5$ [26] and $B_0 = 2 \cdot 10^6$ /ml [25]. (b) Infection speed histograms for the p001 strain of the T7 virus. The other parameter values are $k_1 = 1.29 \cdot 10^{-9}$ ml/min, $\sigma_1 = 0.59 \cdot 10^{-9}$ ml/min, $k_2 = 0.703 \text{ min}^{-1}$, $D_{\text{eff}} = 1.03 \cdot 10^{-2}$ mm²/h, $y = 55.4$ [26] and $B_0 = 2 \cdot 10^6$ /ml [25].

In Fig. 2 we have used a realistic range of k_2 to compare the predictions of several models to experimental data on the front speed. Besides the death rate k_2 , the adsorption rate k_1 also has a substantial uncertainty range (much wider than the rest of the parameters in the system). Thus, in Fig. 3 we analyze the effect of the adsorption rate k_1 on the results of the reaction–diffusion models (for mean values of the remaining parameters). When considering the cohabitation model (shaded gray columns in Fig. 3(a) and (b)), we found the following interesting behavior. As expected intuitively, when k_1 is small the predicted front speed is relatively slow. For example, let us focus on the results for the wild T7 strain in Fig. 3(a): the first and second (from left to right) columns for the cohabitation model were generated by k_1 values within the range $\{\bar{k}_1 - 2\sigma, \bar{k}_1 - 1.5\sigma\} = \{0.11, 0.40\}$ ml/min. These two columns display the slowest speeds in the histogram (specifically, $c \in \{0.12, 0.21\}$ mm/h). This is consistent with the fact that, when $k_1 \rightarrow 0$, the virus is unable to infect cells and cannot produce plaques. However, when increasing the value of k_1 we observed a rapid saturation of the front speed. This effect explains why we observe thinner (but higher) columns at the right of the cohabitation histogram: for k_1 values within the range $\{\bar{k}_1 - \sigma, \bar{k}_1 + 3\sigma\} = \{0.70, 3.06\}$ ml/min, the predicted speed is located in a very thin range (namely, $c \in \{0.23, 0.25\}$ mm/h). This saturation effect indicates that, for high enough values of k_1 , the infection front speed is independent of k_1 . The physical reason is that if virus adsorption into the host cell is very fast, the effect of the characteristic adsorption time (or, equivalently, of its rate k_1) on the infection speed becomes irrelevant as compared to the effect of the diffusion delay time T . This independence of the infection speed on k_1 is also observed for infection fronts of the p001 strain (Fig. 3(b)). Furthermore, for both T7 strains the cohabitation model leads to more realistic results than the YM classical (i.e. noncohabitation) models (Fig. 3(a) and (b)).

To summarize, in Figs. 2 and 3 we have shown that the cohabitation model predicts much better the infection speeds of T7 virus strains than classical noncohabitation models. Moreover, we have seen that the infection speed reaches a saturation

value when increasing the value of the adsorption rate k_1 . In contrast to this relative independence between k_1 and the infection speed, the death rate k_2 (which is strongly correlated to the delay T) has a strong influence on the infection speed (compare the width of the highest columns in Fig. 2 with the width of the highest columns in Fig. 3 for the cohabitation model).

5. Conclusions

In this paper we have presented a model based on cohabitation equations for focal infection systems. According to the cohabitation reaction–diffusion equations, viral particles do not diffuse away from the cell they infect until the cell death takes place and the viral progeny is released into the extracellular medium. This improves the mathematical description of the system in previous models.

We have analyzed the importance of two relevant parameters of the system, namely, the adsorption rate and the death rate. Among these two parameters, the death rate plays a remarkably more important role in determining the speed of the front. When comparing the results of our model with the observed data, we have seen that for two T7 strains the cohabitation model leads to remarkably better results than classical models.

Acknowledgments

We thank the members of the Complex Systems Laboratories for useful discussions. This work was supported by grants from the Fundacion Botin, the MICINN-FEDER (projects SimulPast-Consolider-CSD-2010-00034 and FIS-2009-13050 and FIS-2012-31307) and by the Generalitat de Catalunya (Grup consolidat 2009-SGR-374).

References

- [1] J. Fort, V. Méndez, *Rep. Progr. Phys.* 65 (2002) 895.
- [2] W. van Saarloos, *Phys. Rep.* 386 (2002) 29.
- [3] S.A. Gourley, J.W.-H. So, J.H. Wu, *J. Math. Sci.* 124 (2004) 5119.
- [4] J. Fort, T. Pujol, *Rep. Progr. Phys.* 71 (2008) 086001.
- [5] S.J. Di Bartolo, A.T. Dorsey, *Phys. Rev. Lett.* 77 (1996) 4442.
- [6] T. Pujol, B. Comas, *Phys. Rev. E* 84 (2011) 026306.
- [7] J. Fort, V. Méndez, *Phys. Rev. Lett.* 89 (2002) 178101.
- [8] J.M. Los, P. Golec, G. Węgrzyn, A. Węgrzyn, M. Los, *Appl. Environ. Microbiol.* 74 (16) (2008) 5113.
- [9] S.T. Abedon, R.R. Culler, *J. Theor. Biol.* 248 (2007) 111.
- [10] L.J. Alvarez, P. Thomen, T. Makushok, D. Chatenay, *Biotechnol. Bioeng.* 96 (3) (2007) 615.
- [11] L. Kaliniene, V. Klauska, L. Truncaite, *Arch. Virol.* 155 (2010) 871.
- [12] A. Hofacre, D. Wodarz, N.L. Komarova, H. Fan, *Virology* 423 (2012) 89.
- [13] D.R. Amor, J. Fort, Lag-driven motion in front propagation, *Physica A* (2013) <http://dx.doi.org/10.1016/j.physa.2013.06.058>.
- [14] D.R. Amor, J. Fort, *Phys. Rev. E* 82 (2010) 061905.
- [15] J. Yin, J.S. McCaskill, *Biophys. J.* 61 (1992) 1540.
- [16] N. Isern, J. Fort, *Phys. Rev. E* 80 (2009) 057103.
- [17] H. Fricke, *Phys. Rev.* 24 (1924) 575.
- [18] J. Fort, J. Pérez-Losada, N. Isern, *Phys. Rev. E* 76 (2007) 031913.
- [19] L. Haseltine, V. Lam, J. Yin, J.B. Rawlings, *Bull. Math. Biol.* 70 (2008) 1730.
- [20] J. Fort, V. Méndez, *Phys. Rev. Lett.* 82 (1999) 867.
- [21] N. Isern, J. Fort, J. Pérez-Losada, *J. Stat. Mech. Theory Exp.* (2008) P10012.
- [22] U. Ebert, W. van Saarloos, *Physica D* 146 (2000) 1.
- [23] D.G. Aronson, H.F. Weinberger, *Adv. Math.* 30 (1978) 33.
- [24] J. Fort, *J. Appl. Phys.* 101 (2007) 094701.
- [25] J. Yin, *J. Bacteriol.* 175 (5) (1993) 1272.
- [26] The value of the yield for the wild strain of the T7 was derived in Ref. [7] from observed data. For the case of the p001 mutant, the yield has been obtained from the data in Fig. 3 in Ref. [25], using the same method that was used to derive the yield of the wild strain in Ref. [7].